Journal of Materials Science: Materials in Medicine (2019) 30:23
https://doi.org/10.1007/s10856-019-6223-0

TISSUE ENGINEERING CONSTRUCTS AND CELL SUBSTRATES

Original Research

Synthesis of SiO_2 nanostructures from *Pennisetum glaucum* and their effect on osteogenic differentiation for bone tissue engineering applications

Jegan Athinarayanan[1] · Vaiyapuri Subbarayan Periasamy[1] · Akram Ahmed Qasem[1] · Reshod A. Al-Shagrawi[1] · Ali A. Alshatwi[1]

Received: 2 July 2018 / Accepted: 14 January 2019 / Published online: 12 February 2019

Abstract

Silica nanostructures were fabricated from *Pennisetum glaucum* (pearl millet) seed husk by acid-pretreatment and calcination. The fabricated silica nanostructure (SN) functional groups, crystalline nature, surface morphology, and particle size were analyzed by Fourier transform infrared spectroscopy, X-ray diffraction, scanning electron microscopy, and transmission electron microscopy, respectively. Additionally, the cytocompatibility of SNs was analyzed on human mesenchymal stem cells (hMSCs) in an MTT assay, propidium iodine (PI) staining, and acridine orange/ethidium bromide (AO/EB) staining. We observed peaks at 1090 and 800 cm^{-1}, which were assigned to symmetric, asymmetric, and bending vibrations of O–Si–O. The SNs showed an amorphous nature with a spherical shape and were 20–60 nm in diameter. The MTT assay results indicated that SNs exhibited cytocompatibility in hMSCs. The PI staining and AO/EB staining results suggested that SNs do not affect nuclear morphology at up to 400 µg/mL. Furthermore, SNs effect on osteogenic differentiation in hMSCs was studied. These results indicate that SNs induced osteogenic differentiation in hMSCs by upregulation of ALP, BSP, ON and RUNX2 genes. Our process could valorize the *Pennisetum glaucum* agricultural residues to high value products for bone tissue engineering applications.

Graphical Abstract

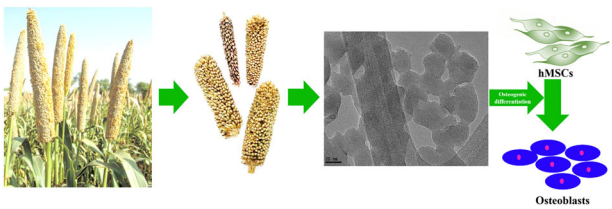

1 Introduction

Nanoscience and technology progress has resulted in revolutionary advancements in different sectors using nanostructured materials with extraordinary optical, electrical, catalytic, magnetic, anti-microbial, anti-oxidant, and anti-cancer properties [1–3]. Nanostructured materials (NMs) are the building blocks of nano-systems, and NM synthesis is a major research field in nanoscience and technology. Various types of NMs have been fabricated using different approaches [4–6]. Among NMs, silica nanostructures have been applied for various purposes. Silica (SiO_2) is the second most abundant material in the

✉ Ali A. Alshatwi
nano.alshatwi@gmail.com
alshatwi@ksu.edu.sa

[1] Nanobiotechnology and Molecular Biology Research Laboratory, Department of Food Science and Nutrition, College of Food and Agricultural Sciences, King Saud University, Riyadh 11451, Saudi Arabia

biosphere, which has been widely examined in the research and development fields of different industries because of their high availability and cost-effectiveness. Silica has widely used in various applications such as electronics, gene delivery, drug delivery, ceramics, thin film substrates, scaffolds, sensors, bio-imaging, catalyst, food packaging, and solar cells [7–11]. Several methods have been used to prepare silica nanoparticles (SNPs), including reverse microemulsion, surfactant template method, sonochemical, sol-gel process, vapor-phase reaction, flame synthesis, and thermal decomposition [10, 12, 13]. On the large-scale, SNs are synthesized using sodium silicate as a precursor. The sodium silicate is prepared by smelting quartz sand in the presence of sodium carbonate at 1300 °C, which requires a large amount of energy [14]. However, these synthetic methods are costly and time-consuming and use hazardous chemicals, limiting their applicability.

The synthesis of NMs from agricultural residues can be applied as a sustainable methodology that can reduce environmental contamination and increase the value of agricultural residues. Silica accumulates in many plant systems (stem, leaves, and root) in a solid form and provides mechanical strength as well as resistant against fungal diseases [15]. Silica phytoliths in the plant epidermal cell wall have different morphologies such as bowls, saddles, dumbbells, boats, and shark sword [15]. The silica content of plant biomass varies, with a high content found in monocots (Cyperaceae family, Commelinaceae family, and Poaceae family) and fern (Equisetaceae family) [16]. Thus, silicified plant biomass may act as a biogenic silica precursor. Interestingly, silica nanostructures derived from plant biomasses have received great attention because their precursors are readily available and because of their sustainability, renewability, and cost-effectiveness [1–3, 15, 17, 18]. Additionally, several plant biomass-based agricultural residues have been utilized as precursors for silica nanostructure fabrication; these plant biomasses include rice husk, rice straw, corn cob, wheat straw, wheat husk, bamboo leaves, sugarcane bagasse, and sorghum bagasse [1–3, 17–23]. *Pennisetum glaucum* (pearl millet) belongs to the Poaceae family, which grows widely on the Africa and Asia continents. Because of the production of pearl millet, very large amounts of pearl millet agricultural residues are generated. However, pearl millet seed husk usage is very low because of its adverse properties including high ash content, degradation resistance and low nutritive value. The large quantity of the residues are not utilizing properly, which are burning in open air that result emission of greenhouse gases that leads environmental pollution. In this study, we analyzed the applications of agricultural byproducts and reduction of environmental pollution caused by their disposal. We used pearl millet agricultural residues as a sustainable resource for silica nanostructure (SN) fabrication for various biomedical applications.

2 Materials and methods

2.1 Materials

Pennisetum glaucum seed husk was collected from a local market in Riyadh, Kingdom of Saudi Arabia. Hydrochloric acid was purchased from Merck (Kenilworth, NJ, USA). Dulbecco's modified eagle medium, MTT (3-(4,5-dimethylthiazol-2-yl)−2,5-diphenyltetrazolium bromide), propidium iodide, acridine orange, and ethidium bromide were obtained from Thermo Fisher Scientific (Waltham, MA, USA).

2.2 Synthesis of silica nanostructures

Approximately 10 g of *P. glaucum* seed husk was mixed with 200 mL of 0.1 M hydrochloric acid and incubated at 120 °C for 2 h under 15 lbs pressure using an autoclave. After acid pretreatment, the *P. glaucum* seed husk residues were washed with distilled water until HCl was completely removed. The obtained residues were calcinated at different temperatures (500 °C, 600 °C, and 700 °C) for 1 h using muffle furnace. The acid pretreated seed husk containing organic substances were removed by thermal decomposition. After calcination of the residues, we obtained clear white silica nanostructures powder, which was subjected to characterization.

2.3 Characterization

The functional group of the *P. glaucum* seed husk and derived SNs were analyzed by Fourier transformation infrared (FTIR) spectroscopy (Nicolette Nexus 470, USA). An X-ray diffractometer (Cu Kα radiation = 1.5406 Å) was used to investigate the crystalline properties of the prepared SNs. The shape and size of the prepared SNs were investigated by scanning electron microscopy (SEM) and transmission electron microscopy (2010F, Jeol, Tokyo, Japan). For transmission electron microscopy (TEM) analysis, the sample was dispersed in ethanol and coated on carbon-coated copper grids.

2.4 Cell viability assay

Human bone marrow derived human mesenchymal stem cells were obtained as a gift from Stem cell unit (College of medicine, King Saud University, Riyadh, Kingdom of Saudi Arabia). The human mesenchymal stem cells were

used as an in vitro model for cytocompatibility analysis. The cells were grown in T-25 flasks using Dulbecco's modified eagle medium supplemented with 10% fetal bovine serum and 1% antibiotics at 37 °C under 5% CO_2. The effect of prepared SNs on cell viability of hMSCs was assessed in MTT assay [24]. Approximately 10,000 cells per well were plated in 96-well pates and incubated in a CO_2 incubator. The SNs were dispersed in cell culture media and used for all in vitro assays. After overnight incubation, the cells were exposed to SNs with different concentrations (0, 25, 50, 100, 200, and 400 µg/mL) for 24 and 48 h. After incubation, 20 µL of 5 mg/mL MTT was added to each well. The plate was kept in dark for 6 h at 37 °C. The plate was read using a Bio-Rad microplate reader (Hercules, CA, USA) at 570 nm (measurement filter) and 630 nm (reference filter). The obtained data was used to calculate the percentage of cell viability with the following formula:

$$\text{Cell viability } (\%) = \frac{\text{Mean OD of untreated cells (control)} - \text{Mean OD of treated cells}}{\text{Mean OD of untreated cells (control)}} \times 100$$

2.5 PI staining

The hMSCs was seeded at a density of 50,000 cells per well in a 24-well plate. After overnight incubation, the cells were treated with different doses of SNs for 24 and 48 h. After incubation, the cells were fixed with ice cold 70% ethanol and stained with PI for 15 min. The cells were washed with phosphate-buffered saline and examined under a fluorescence microscope.

2.6 AO/EB staining

The hMSCs was seeded at a density of 50,000 cells per well in a 24-well plate. After overnight incubation, the cells were treated with different doses of SNs for 24 and 48 h. After incubation, the cells were stained with AO/EB (Acridine orange/Ethidium bromide) dual stain for 5 min. After staining, the cells were examined under a fluorescence microscope.

2.7 Osteogenic induction

The osteoblast differentiation of hMSCs in the presence of SNs was analyzed using alizarin red S staining. The 1×10^4 cells per well was seeded in 24 well plates. After 24 h incubation, the cells were growing in osteogenic differentiation media with different concentration of SNs (0, 12.5, 25, 50, 100, 200 µg/mL). Every 3 days osteoblast differentiation media was replaced and the cells were treated with SNs. After 14 days incubation, the mineralized nodules were observed using alizarin red S staining. The cell culture medium was removed and washed with cold-PBS. Then, the cells were fixed with 70% cold-ethanol at room temperature and cells were washed with distilled water. After the cell fixation, cells were stained with alizarin red S (40 mM) for 15 min at room temperature. After incubation, cells were washed with distilled water for thrice. Consequently, mineralized nodules were observed by naked eye and bright-field microscope.

2.8 Quantitative real-time PCR analysis of gene expression

The SNs effect on gene expression of hMSCs was studied using reverse transcription PCR (RT-PCR; Applied Biosystems 7500 Fast, Foster City, CA) using a real-time SYBR Green/ROX gene expression assay kit from QIAGEN (Hilden, Germany). cDNA was directly prepared from cultured cells using a Fastlane® Cell cDNA kit from QIAGEN (Hilden, Germany), and the mRNA levels of osteoblast specific marker genes alkaline phosphatase (ALP), bone sialoprotein (BSP), RUNX2 and osteonectin (ON) and the reference gene, glyceraldehyde 3-phosphate dehydrogenase (GAPDH), were assayed using gene-specific SYBR Green-based QuantiTect® Primer assays from QIAGEN (Hilden, Germany). Quantitative real-time RT-PCR was performed in a reaction volume of 25 µL in accordance with the manufacturer's instructions. Briefly, 12.5 µL of the master mix, 2.0 µL of assay primers (10 ×) and 10 µL of template cDNA (100 ng) were added to each well. After a being centrifuged briefly, the plate was subjected to PCR under the following conditions: (i) activation at 95 °C for 5 min, followed by 40 cycles of (ii) denaturation at 95 °C for 5 s and (iii) annealing/extension at 60 °C for 30 s. All samples and controls were run in triplicate on an AB7500 Fast Real-Time PCR system. The quantitative RT-PCR data were analyzed using a comparative threshold (Ct) method, and the fold inductions of the samples were compared with those of the untreated samples. The GAPDH was used as an internal reference gene to normalize the expression of the osteoblast specific marker genes. The Ct cycle was used to determine the expression level in the control and in hMSCs treated with SNs. The gene expression level was then calculated as previously described by Alshatwi et al. [2]. The results are expressed as the ratio of the reference gene to the target gene as calculated by the following formula: $\Delta Ct =$ Ct (target genes)-Ct (GAPDH). To determine the relative expression level, the following formula was used: $\Delta\Delta Ct =$ ΔCt (Treated) $- \Delta Ct$ (untreated control). Thus, the expression levels are expressed as n-fold differences relative to the reference gene. This value was used to plot the expression of antioxidant enzyme genes using the mathematical expression $2^{-\Delta\Delta Ct}$.

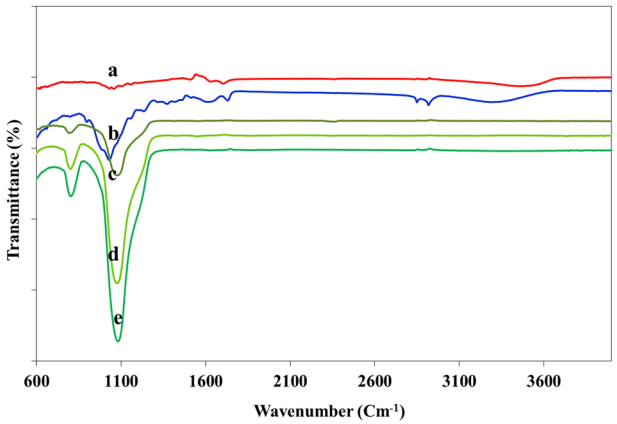

Fig. 1 FT-IR spectra of **a** pearl millet seed husk, **b** acid-treated pearl millet seed husk, and silica nanostructures obtained at different calcination temperatures of **c** 500 °C, **d** 600 °C, and **e** 700 °C

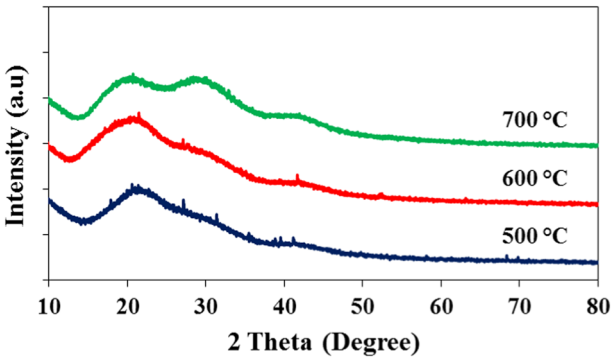

Fig. 2 X-ray diffractograms of **a** pearl millet seed husk, **b** acid-treated pearl millet seed husk, and silica nanostructures obtained at different calcination temperatures of **c** 500 °C, **d** 600 °C, and **e** 700 °C

2.9 Statistical analysis

The presented results were obtained from three independent experiments. The Microsoft Excel software (Microsoft Corp., KY, USA) was used to calculate the respective mean, standard deviation and *t*-test. For all comparisons, differences were considered statistically significant at $p < 0.05$.

3 Results

3.1 Synthesis of silica nanostructures

The *P. glaucum* (pearl millet) seed husk was utilized as a precursor for silica nanostructure fabrication. The residues were pretreated with hydrochloric acid to eliminate metal ions and initiate lignocellulosic biomass degradation. The calcination process completely removed organic substances from the residues, resulting in the production of white color silica nanostructures. Fig. 1 shows the FTIR spectra of the fabricated SNs. The raw and acid-pretreated pearl millet seed husk showed numerous absorption peaks assigned to organic (cellulose, lignin, and hemicellulose) and inorganic (SiO_2) substances. In contrast, peaks related to organic substances disappeared in the synthesized SNs, suggesting that the calcination process completely removed the organic substances. Interestingly, we observed peaks at 1100 and 800 cm^{-1}, which were assigned to symmetric, asymmetric, and bending vibrations of O–Si–O. The absorption peaks of synthesized SNs using different calcination temperatures were identical. The FTIR spectra clearly indicated that SNs were pure and no organic substances were present on the prepared samples. Fig. 2 shows the X-ray diffraction pattern (XRD) of SNs obtained from pearl millet seed husk at different calcination temperatures. The XRD pattern showed the broad peak near a 2θ value of 22°, confirming that the SNs were amorphous in nature at the nanoscale level. The XRD results for all samples were identical, and no impure peaks were observed. The surface morphology of the prepared SNs was analyzed by SEM. Fig. 3 shows the SEM images of SNs, which clearly reveal the prepared SNs have aggregation and clusters of spherical particles. At low magnification of SEM images, crumbled structures were observed in all SNs samples. Interestingly, we observed the agglomeration of spherical and irregular particles in SEM images at high magnification. The TEM images clearly indicated that silica nanostructures were spherical in shape with agglomeration and a diameter of 20–60 nm (Fig. 4). When the calcination temperature was changed, SN morphology also differed, suggesting that the calcination temperature affects nanostructure morphology.

3.2 Cytocompatibility assessment

The cytotoxic properties of SNs were evaluated using human mesenchymal stem cells as an in vitro model. The hMSCs were treated with different concentration of SNs for 24 and 48 h (Fig. 5). The high concentration of the SNs slightly reduced the cell viability of hMSCs, but low concentration of SNs caused no changes in cell viability. Additionally, cell viability was reduced by 5–7% in hMSCs, even at 400 µg/mL of SN treatment. Our results suggest that SNs are non-toxic and biocompatible. The cellular and nuclear morphology of hMSCs is shown in Fig. 6. We observed elongated, needle-shaped, and healthy cells in the control group. Additionally, the same morphological features were observed in treated cells, clearly suggesting that SNs do not disturb the cellular morphology of hMSCs even at high concentrations in the SN-treated group. Whether SNs induce cell death through apoptosis or other pathways was studied by AO/EB dual staining (Fig. 6). In AO/EB stained cells, we observed no features related to apoptosis, necrosis, necroptosis, or autophagy. In contrast, we observed healthy cells with intact nuclei in both control and

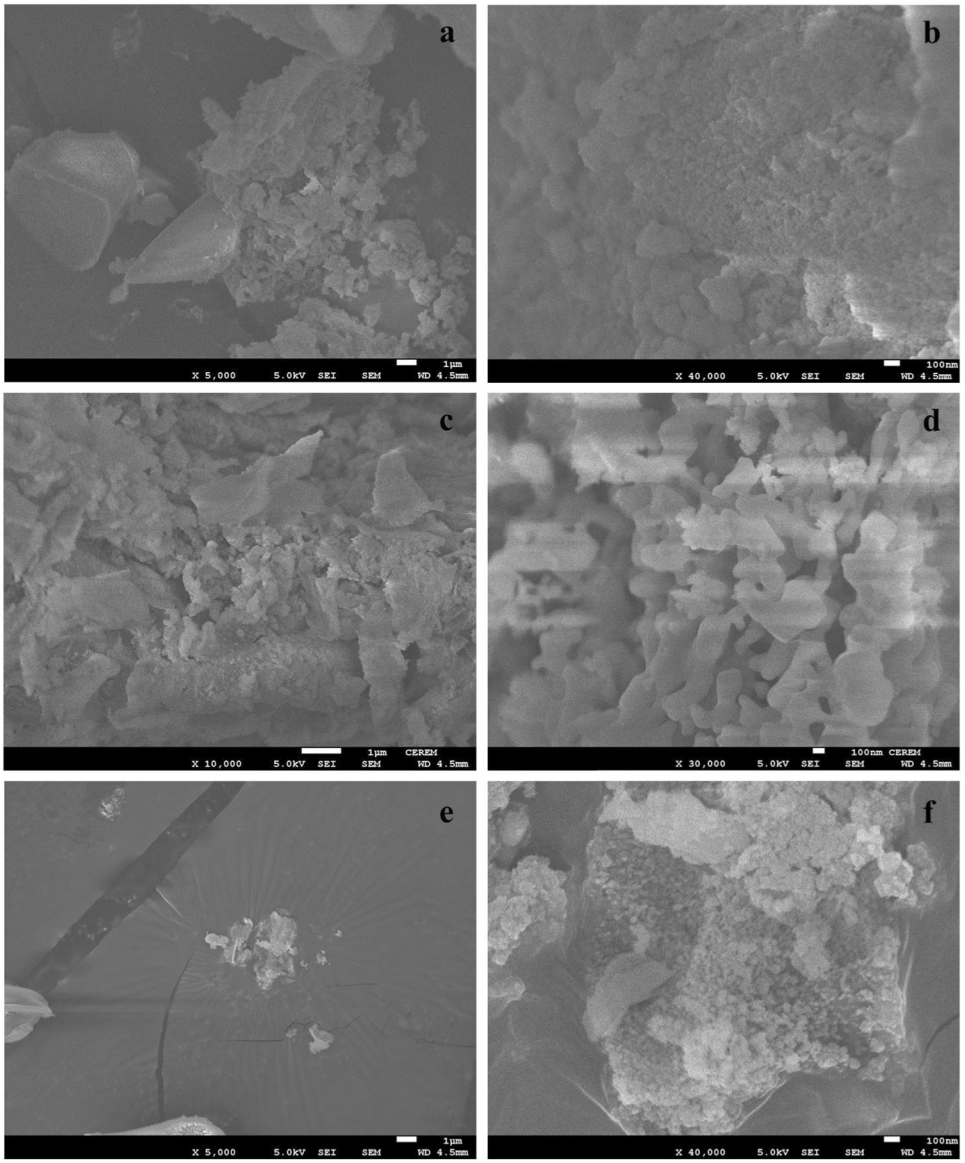

Fig. 3 Scanning electron microscopic images of silica nanostructures obtained from pearl millet seed husk using different calcination temperatures **a**, **b** 500 °C, **c**, **d** 600 °C and **e**, **f** 700 °C

SN-treated hMSCs. Thus, the SNs are highly suitable for biological applications. Furthermore, we analyzed the nuclear morphological changes in SN-treated cells by PI staining (Fig. 7). The results revealed cells with intact nuclei in the control group and SN-treated group, which clearly indicated SN compatibility, benignness, and beneficiary behavior on hMSCs.

3.3 Osteogenic differentiation

Silica plays an important beneficial role in bone health and bone development. In this study, we have investigated the role of plant derived SNs on osteogenic differentiation at molecular level. The hMSCs treated with different concentration of the SNs for 14 days to study the effect of SNs on osteogenic differentiation of human mesenchymal stem cells. After 14 days SNs exposure, we assessed the calcium mineralization using Alizarin red staining that is used to prove the calcium deposition and nodules formation. The alizarin red S can selectively associate with calcium ions and produce orange red precipitate. Fig. 8 depicts Alizarin red staining images of human mesenchymal stem cells after culturing in osteogenic differentiation media at 14 days. We observed the mineralized calcium deposition and bone nodules in SNs treated and untreated hMSCs, which indicates hMSCs are differentiate into osteoblast lineage. To compare with control, large amount of bone like nodules are found in SNs treated cells. Moreover, the amount of calcium deposition and nodules formation increased by dose-dependent manner. Interestingly, 200 µg/mL SNs

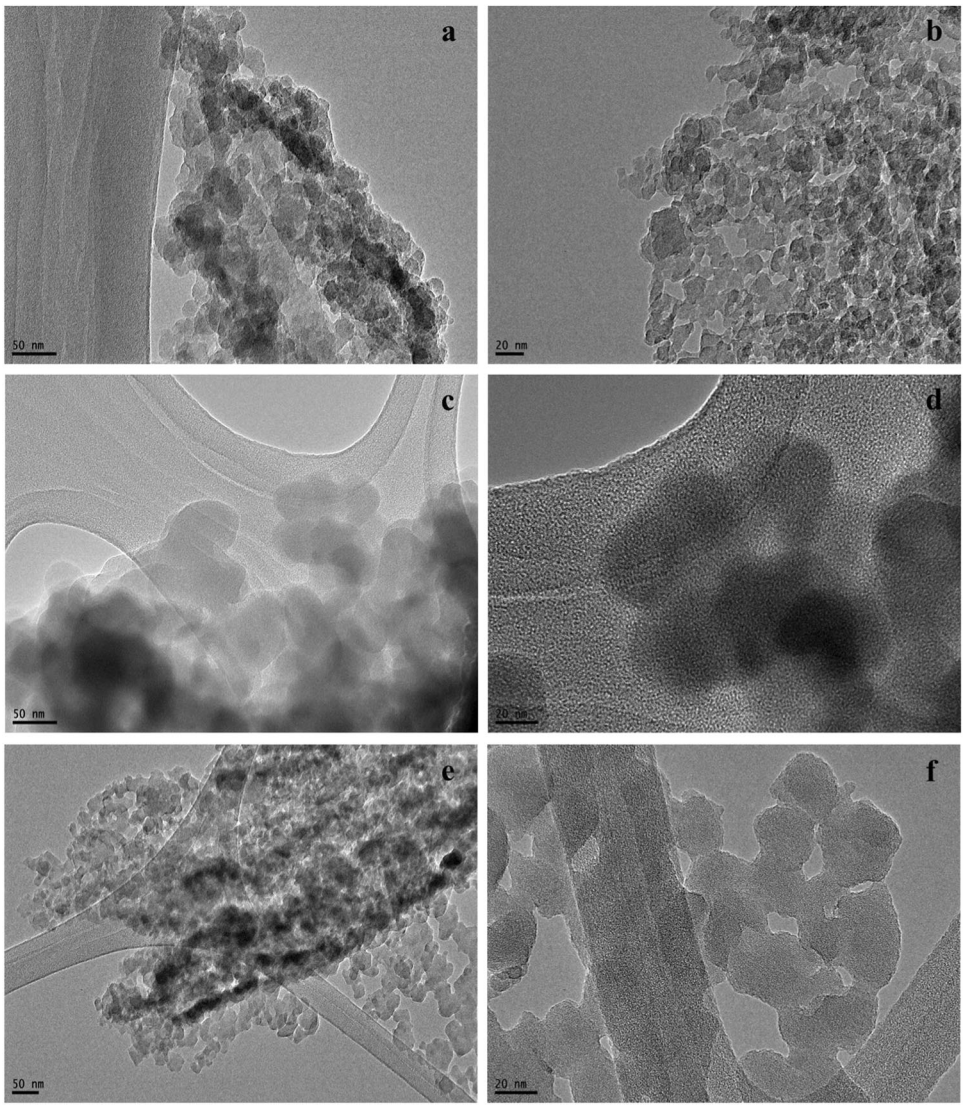

Fig. 4 Transmission electron microscopic images of silica nanostructures obtained from pearl millet seed husk using different calcination temperatures **a**, **b** 500 °C, **c**, **d** 600 °C and **e**, **f** 700 °C

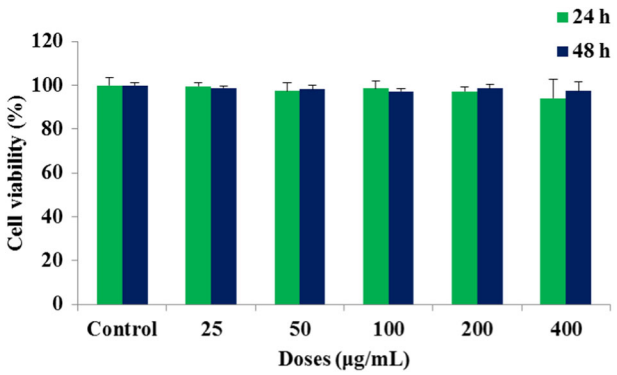

Fig. 5 Influence of silica nanostructures on human mesenchymal stem cell viability

significantly promotes the nodules formation. These results clearly suggested that SNs can induce the calcium deposition and nodules formation osteogenic differentiation in hMSCs.

3.4 Osteogenic markers expression

The SNs influence of osteogenic differentiation was studied at molecular level by gene expression analysis using RT-PCR. The marker gene of osteogenic differentiation including ALP, RUNX2, ON and BSP expression is analyzed. The ALP is an early marker of osteogenic differentiation, during matrix maturation process ALP expression gradually improved to optimum, and its expression level is decreased at matrix mineralization. The gene expression of ALP, RUNX2, ON and BSP are plotted in Fig. 9. At 14 days, the ALP gene expression significantly increased in SNs treated cells than control. Interestingly, the expression level of ALP is gradually increased in SNs treated cells by dose-dependent manner. Our results demonstrated that SNs significantly induce osteogenic differentiation in hMSCs. Bone sialoprotein (BSP) gene expression level is higher in SNs treated cells than control. In high concentration of SNs exposed cells has 6 folds was

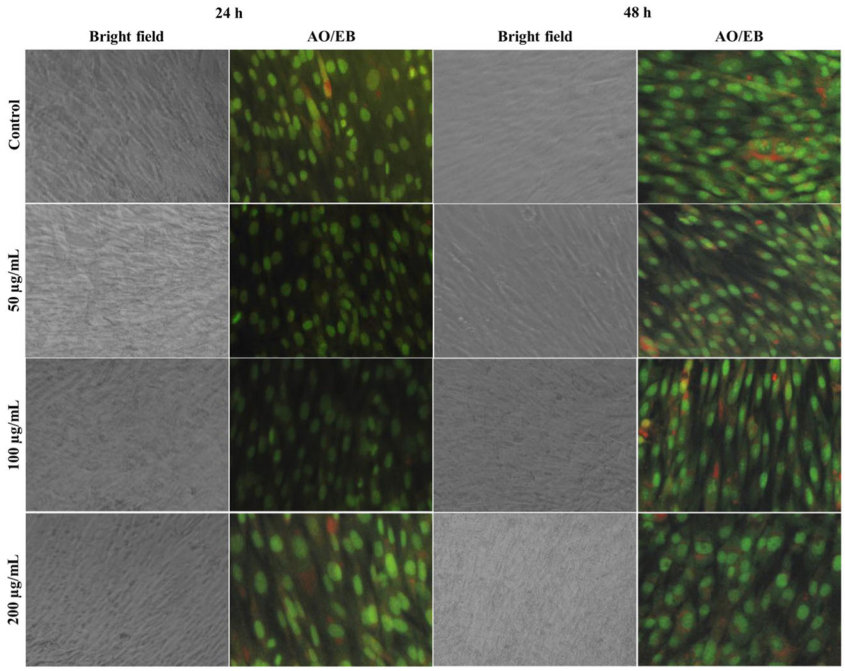

Fig. 6 Silica nanostructure effect on cellular and nuclear morphology of human mesenchymal stem cells

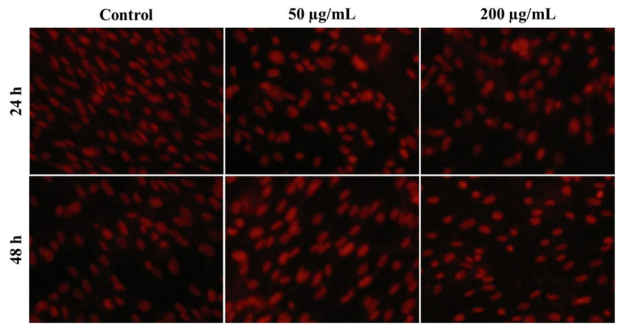

Fig. 7 Influence of silica nanostructures on human mesenchymal stem cell nuclear morphology determined by PI staining

observed in BSP expression. RUNX2 (Runt-related transcription factor 2) is referred as core-binding factor subunit alpha-1 (CBF-alpha-1) protein. Earlier studies suggested that RUNX2 gene expression has upregulated in preosteoblasts, and plays a key role in bone formation. Although, RUNX2 expression is down regulated in matured osteoblasts. In this study, RUNX2 expression is significantly upregulated in SNs exposed human mesenchymal stem cells at 14 days and its expression level is increased by dose-dependently. Osteonectin (ON) is a glycoprotein that secretes during bone mineralization. Moreover, osteonectin plays a crucial role in collagen affinity, bone mineralization and cell-matrix communication. The ON gene expression level has no significance observed in low concentration SNs treated cells, but remarkable fold changes found in 200 µg/mL SNs treated cells than control. Over all gene expression results strongly indicates that SNs triggers osteogenic differentiation in human mesenchymal stem cells.

4 Discussion

Because of the silicification process, silica phytoliths accumulates in plant bodies. These plant-based agricultural residues contain a huge quantity of silica. In this regard, several studies have attempted to fabricate silica nanostructures using different types of agricultural residues such as sorghum bagasse, sugarcane bagasse, wheat straw, corn cob, bamboo leaves, rice straw, wheat husk, and rice husk [1–3, 17–23]. However, *P. glaucum* (pearl millet) seed husk has not been used for SN preparation. Thus, we used pearl millet seed husk as a precursor for SN fabrication. The usage of cheap, sustainable and renewable *Pennisetum glaucum* (pearl millet) seed husk can be considered as a bioprecursor for biogenic silica nanostructures. Pearl millet seed husks contain 9.1% silica; compared to other agricultural residues, pearl millet husk contains a high amount of biogenic silica [1, 21, 25–31]. The FTIR spectra of the prepared SNs displayed a peak corresponding to symmetric, asymmetric, and bending vibration of O–Si–O at 1100 and 800 cm^{-1}. Similarly, previous studies reported that silica nanoparticles exhibited a characteristic absorption band at approximately 1103 and 804 cm^{-1} [21, 29, 32]. Previous studies demonstrated that the calcination temperature influences the SN crystallization process [21, 33]. Interestingly, crystallization that occurs in amorphous silica is based on the calcination temperature and time. A calcination temperature greater than 700 °C enhances crystallization [21, 33, 34]. Thus, in this study we used a calcination temperature of 500–700 °C. XRD revealed a

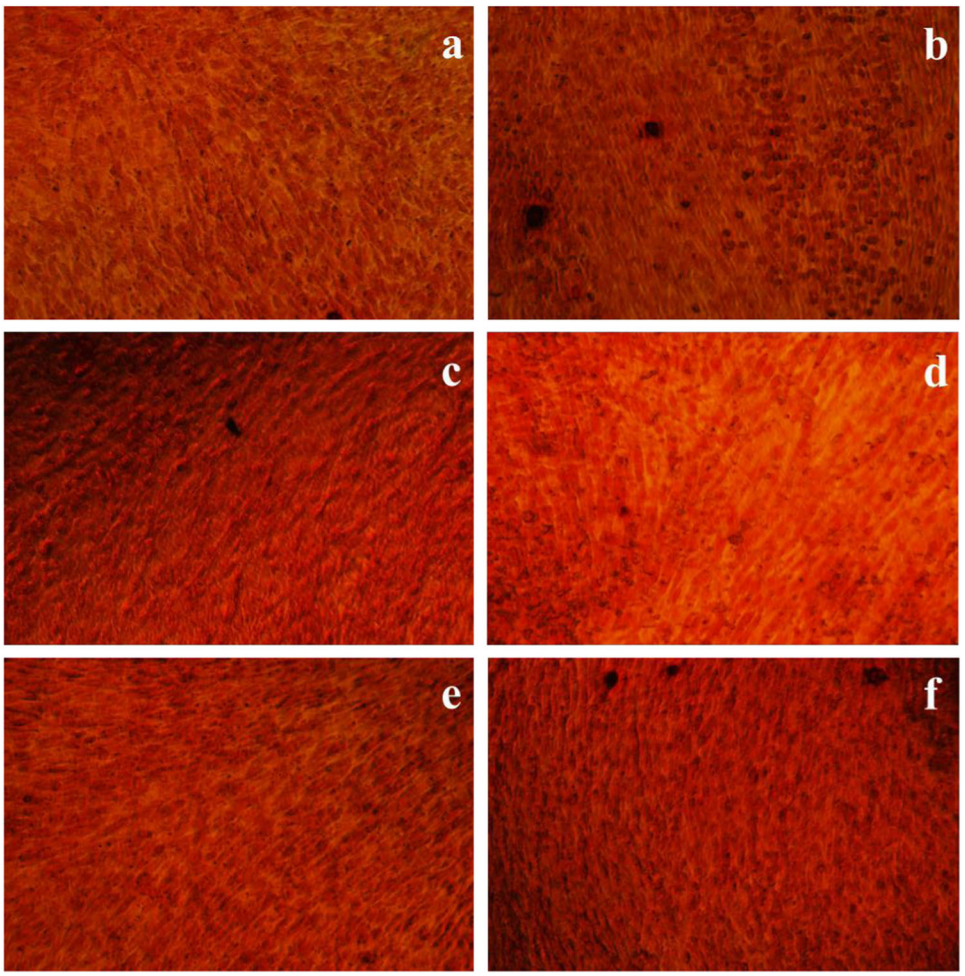

Fig. 8 Effect of synthesized SNs on bone mineralization. The calcium deposition was stained using Alizarin Red S on day 14. **a** At day 14, hMSCs able to produce mineralized matrix in osteoconductive media (Control). **b** 12.5 µg/mL, **c** 25 µg/mL, **d** 50 µg/mL, **e** 100 µg/mL and **f** 200 µg/mL SNs triggered calcium nodules formation by dose-dependently

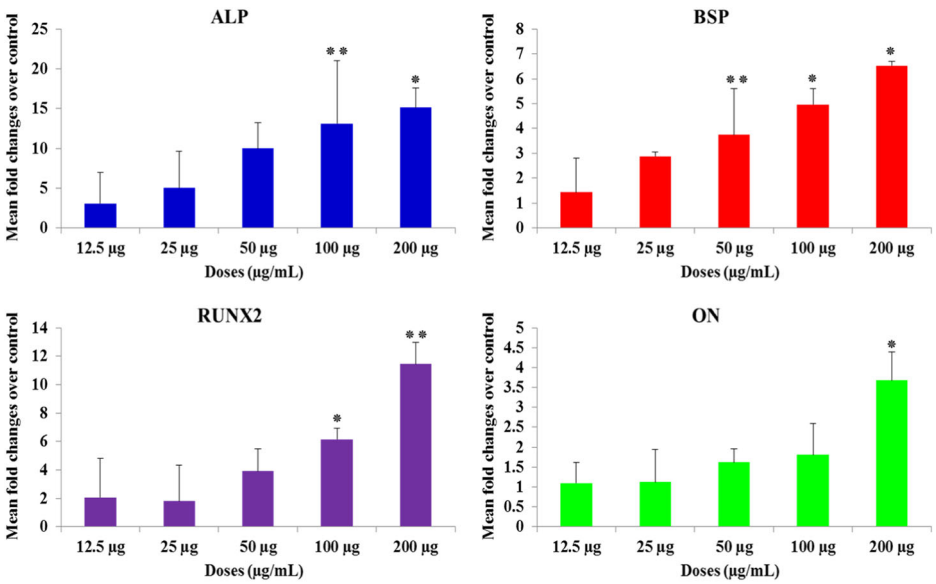

Fig. 9 RT-PCR gene expression analysis results of osteogenesis associated markers after hMSCs were exposed to different concentration of SNs for 14 days. The markers including alkaline phosphatase (ALP), Bone sialoprotein (BSP), Runt-related transcription factor 2 (RUNX2) and Osteonectin (ON). Glyceraldehyde 3-phosphate dehydrogenase (GAPDH) was used as the endogenous control. (*$P > 0.005$ and **$P > 0.05$)

broad peak at a 2θ value of 22°, indicating that the SNs had an amorphous nature [1, 29]. Morphological analysis revealed SN clusters of 20–60 nm and aggregated, spherical particles. The morphology of SNs showed slight differences based on the calcination temperature. The particle size of SNs has increases with calcination temperature.

At high calcination temperature, we found the agglomeration in the formed SNs due to high surface activity at nanoscale regime. Earlier studies demonstrated that high temperature initiate recrystallization and growth of particles [35].

Affandi et al. reported that spherical silica nanoparticles were synthesized from rice husk [27]. Additionally, Sankar et al. synthesized clusters of spherical silica nanoparticles that were 10–50 nm in diameter [25]. For biomedicine and food sector applications, materials must be non-toxic and compatible with cell and tissue properties. We analyzed the cytotoxic properties of synthesized SNs using an in vitro approach. Our previous study demonstrated that biogenic silica nanoparticles obtained from rice husk exhibited biocompatibility against human lung fibroblast cells [2]. Additionally, sugarcane bagasse-derived silica nanoparticles do not exhibit toxic effects on human lung fibroblast cells [3]. Similarly, in the present study, pearl millet-derived SNs exhibited biocompatibility with human mesenchymal stem cells. Earlier studies demonstrated that high silica intake increase the bone mineral density and silica deficiency triggers reduction of bone mineral density, decrease the mineral content and enhances the collagen breakdown [36]. Jugdaohsingh et al. study suggested that dietary silica intake increase the bone mineral density in hip site of men and premenopausal women [37]. Several studies suggested that biocompatible silica nanoparticles induced osteogenic differentiation and increased bone strength [38, 39]. A number of previous studies have investigated silica based materials role on osteogenic differentiation. Gaharwar et al demonstrated that biocompatible synthetic silicate strongly enhanced progressive pattern of osteogenic differentiation through upregulation of ALP and RUNX2 gene expression [40]. Orthosilicic acid (H_4SiO_4) increase the alkaline phosphatase activity and promotes collagen type I synthesis in osteoblasts [39]. Wang et al. demonstrates that porous β-calcium silicate/Poly-D,L-Lactide-Glycolide scaffold promotes bone regeneration in rabbit and osteogenic differentiation in mesenchymal stem cells through AMPK/Erk1/2 signaling pathway [41]. Jiao et al reported that silica and appetite mineralized collagen scaffold enhanced osteogenic differentiation by increase the alkaline phosphatase activity, triggers mineralization process and osteoblast selective markers expression [42]. Our study results clearly demonstrated that SNs induced osteogenic differentiation. Thus, the SNs may be applicable for bone tissue engineering and as food supplements. However, in vivo studies also necessary to implement the SNs in clinical and food industry applications. Our results clearly suggest that inexpensive pearl millet agricultural residues can be used to produce high-value products for biomedical and food industry applications.

5 Conclusion

We synthesized silica nanostructures using *P. glaucum* (pearl millet) seed husk as a sustainable precursor in a combined process (acid-pretreatment and calcination). Silica nanostructures (SNs) showed an absorption peak at approximately 808 cm^{-1}, which was assigned to stretching of O-Si-O groups. SNs showed an amorphous nature with a nanoscale structure 20–60 nm in diameter. The cell viability assay results suggested that SNs have excellent biocompatibility with hMSCs. Nuclear morphology images indicated that SNs do not induce nuclear morphological changes in hMSCs. Our results clearly suggested that SNs are non-toxic and biocompatible. Thus, the SNs can be applied in biomedical applications such as bone tissue engineering, drug delivery, and bio-imaging.

Acknowledgements We gratefully acknowledge the financial support of the Distinguished Scientist Fellowship Programme, King Saud University, Saudi Arabia. The partial work of this manuscript has achieved a US patent (US patent granted on 2 August 2016, US 9403688 B1).

Compliance with ethical standards

Conflict of interest The authors declare that they have no conflict of interest.

References

1. Athinarayanan J, Periasamy VS, Alhazmi M, Alatiah KA, Alshatwi AA. Synthesis of biogenic silica nanoparticles from rice husks for biomedical applications. Ceram Int. 2015;41:275–81.
2. Alshatwi AA, Athinarayanan J, Periasamy VS. Biocompatibility assessment of rice husk-derived biogenic silica nanoparticles for biomedical applications. Mater Sci Eng C. 2015;47:8–16.
3. Athinarayanan J, Periasamy VS, Alhazmi M, Alshatwi AA. Synthesis and biocompatibility assessment of sugarcane bagasse-derived biogenic silica nanoparticles for biomedical applications. J Biomed Mater Res B. 2017;105:340–9.
4. Reiss P, Carrière M, Lincheneau C, Vaure L, Tamang S. Synthesis of semiconductor nanocrystals, focusing on nontoxic and Earth-abundant materials. Chem Rev. 2016;116:10731–819.
5. Varma A, Mukasyan AS, Rogachev AS, Manukyan KV. Solution combustion synthesis of nanoscale materials. Chem Rev. 2016;116:14493–586.
6. Chen G, Qiu H, Prasad PN, Chen X. Upconversion nanoparticles: design, nanochemistry, and applications in theranostics. Chem Rev. 2014;114:5161–214.

7. Slowing II, Trewyn BG, Giri S, Lin VY. Mesoporous silica nanoparticles for drug delivery and biosensing applications. Adv Funct Mater. 2007;17:1225–36.
8. Li Z, Barnes JC, Bosoy A, Stoddart JF, Zink JI. Mesoporous silica nanoparticles in biomedical applications. Chem Soc Rev. 2012;41:2590–605.
9. Burns A, Ow H, Wiesner U. Fluorescent core–shell silica nanoparticles: towards "Lab on a Particle" architectures for nanobiotechnology. Chem Soc Rev. 2006;35:1028–42.
10. Rahman IA, Padavettan V. Synthesis of silica nanoparticles by sol-gel: size-dependent properties, surface modification, and applications in silica-polymer nanocomposites—a review. J Nanomater. 2012;2012:8.
11. Jeong S, Garnett EC, Wang S, Yu Z, Fan S, Brongersma ML, McGehee MD, Cui Y. Hybrid silicon nanocone–polymer solar cells. Nano Lett. 2012;12:2971–6.
12. Kresge CT, Leonowicz ME, Roth WJ, Vartuli JC, Beck JS. Ordered mesoporous molecular sieves synthesized by a liquid-crystal template mechanism. Nature. 1992;359:710–2.
13. Gholami T, Salavati-Niasari M, Bazarganipour M, Noori E. Synthesis and characterization of spherical silica nanoparticles by modified Stöber process assisted by organic ligand. Superlattices Microstruct. 2013;61:33–41.
14. Liou TH, Yang CC. Synthesis and surface characteristics of nanosilica produced from alkali-extracted rice husk ash. Mat Sci Eng B. 2011;176:521–9.
15. Neethirajan S, Gordon R, Wang L. Potential of silica bodies (phytoliths) for nanotechnology. Trends Biotechnol. 2009;27:461–7.
16. Kumar S, Soukup M, Elbaum R. Silicification in grasses: variation between different cell types. Front Plant Sci. 2017;8:438.
17. Wang W, Martin JC, Fan X, Han A, Luo Z, Sun L. Silica nanoparticles and frameworks from rice husk biomass. ACS Appl Mater Interfaces. 2012;4:977–81.
18. Chen H, Wang W, Martin JC, Oliphant AJ, Doerr PA, Xu JF, DeBorn KM, Chen C, Sun L.Extraction of lignocellulose and synthesis of porous silica nanoparticles from rice husks: a comprehensive utilization of rice husk biomass.ACS Sustain Chem Eng. 2012;1:254–9.
19. Kamiya K, Oka AI, Nasu H, Hashimoto T. Comparative study of structure of silica gels from different sources. J Sol Gel Sci Technol. 2000;19:495–9.
20. Mupa M, Hungwe CB, Witzleben S, Mahamadi C, Muchanyereyi N. Extraction of silica gel from Sorghum bicolour (L.) moench bagasse ash. Afr. J Pure Appl Chem. 2015;9:12–17.
21. Chen H, Wang F, Zhang C, Shi Y, Jin G, Yuan S. Preparation of nano-silica materials: the concept from wheat straw. J Non Cryst Solids. 2010;356:2781–5.
22. Chandrasekhar SA, Satyanarayana KG, Pramada PN, Raghavan P, Gupta TN. Review processing, properties and applications of reactive silica from rice husk—an overview. J Mater Sci. 2003;38:3159–68.
23. Bansal V, Ahmad A, Sastry M. Fungus-mediated biotransformation of amorphous silica in rice husk to nanocrystalline silica. J Am Chem Soc. 2006;128:14059–66.
24. Periasamy VS, Athinarayanan J, Alfawaz MA, Alshatwi AA. Carbon nanoparticle induced cytotoxicity in human mesenchymal stem cells through upregulation of TNF3, NFKBIA and BCL2L1 genes. Chemosphere. 2016;144:275–84.
25. Sankar S, Sharma SK, Kaur N, Lee B, Kim DY, Lee S, Jung H. Biogenerated silica nanoparticles synthesized from sticky, red, and brown rice husk ashes by a chemical method. Ceram Int. 2016;42:4875–85.
26. San NO, Kurşungöz C, Tümtaş Y, Yaşa Ö, Ortaç B, Tekinay T. Novel one-step synthesis of silica nanoparticles from sugarbeet bagasse by laser ablation and their effects on the growth of freshwater algae culture. Particuology. 2014;17:29–35.
27. Affandi S, Setyawan H, Winardi S, Purwanto A, Balgis R. A facile method for production of high-purity silica xerogels from bagasse ash. Adv Polym Tech. 2009;20:468–72.
28. Zaky RR, Hessien MM, El-Midany AA, Khedr MH, Abdel-Aal EA, El-Barawy KA. Preparation of silica nanoparticles from semi-burned rice straw ash. Powder Technol. 2008;185:31–35.
29. Balamurugan M, Saravanan S. Producing nanosilica from Sorghum vulgare seed heads. Powder Technol. 2012;224:345–50.
30. Rangaraj S, Venkatachalam R. A lucrative chemical processing of bamboo leaf biomass to synthesize biocompatible amorphous silica nanoparticles of biomedical importance. Appl Nanosci. 2017;7:145–53.
31. Lu P, Hsieh YL. Highly pure amorphous silica nano-disks from rice straw. Powder Technol. 2012;225:149–55.
32. Liou TH. Preparation and characterization of nano-structured silica from rice husk. Mat Sci Eng A. 2004;364:313–23.
33. Ibrahim DM, Helmy M. Crystallite growth of rice husk ash silica. Thermochim Acta. 1981;45:79–85.
34. Umeda J, Kondoh K. High-purification of amorphous silica originated from rice husks by combination of polysaccharide hydrolysis and metallic impurities removal. Ind Crops Prod. 2010;32:539–44.
35. Goswami PP, Choudhury HA, Chakma S, Moholkar VS. Sonochemical synthesis and characterization of manganese ferrite nanoparticles. Ind Eng Chem Res. 2013;52:17848–55.
36. Sripanyakorn S, Jugdaohsingh R, Thompson RP, Powell JJ. Dietary silicon and bone health. Nutr Bull. 2005;30:222–30.
37. Jugdaohsingh R, Tucker KL, Qiao N, Cupples LA, Kiel DP, Powell JJ. Dietary silicon intake is positively associated with bone mineral density in men and premenopausal women of the Framingham Offspring cohort. J Bone Miner Res. 2004;19:297–307.
38. Keeting PE, Oursler MJ, Wiegand KE, Bonde SK, Spelsberg TC, Riggs BL. Zeolite A increases proliferation, differentiation, and transforming growth factor β production in normal adult human osteoblast-like cells in vitro. J Bone Miner Res. 1992;7:1281–9.
39. Reffitt DM, Ogston N, Jugdaohsingh R, Cheung HFJ, Evans BAJ, Thompson RPH, Powell JJ, Hampson GN. Orthosilicic acid stimulates collagen type 1 synthesis and osteoblastic differentiation in human osteoblast-like cells in vitro. Bone. 2003;32:127–35.
40. Gaharwar AK, Mihaila SM, Swami A, Patel A, Sant S, Reis RL, Marques AP, Gomes ME, Khademhosseini A. Bioactive silicate nanoplatelets for osteogenic differentiation of human mesenchymal stem cells. Adv Mater. 2013;25:3329–36.
41. Wang C, Lin K, Chang J, Sun J. Osteogenesis and angiogenesis induced by porous β-CaSiO3/PDLGA composite scaffold via activation of AMPK/ERK1/2 and PI3K/Akt pathways. Biomaterials. 2013;34:64–77.
42. Jiao K, Niu LN, Li QH, Chen FM, Zhao W, Li JJ, Chen JH, Cutler CW, Pashley DH, Tay FR. Biphasic silica/apatite co-mineralized collagen scaffolds stimulate osteogenesis and inhibit RANKL-mediated osteoclastogenesis. Acta Biomater. 2015;19:23–32.